September 1999 • NREL/SR-520-26382

Subcontractor Report

In-Situ Sensors for Process Control of CuIn(Ga)Se_2 Module Deposition

Annual Technical Report
15 February 1998—15 February 1999

I.L. Eisgruber, T.L. Wangensteen, C. Marshall, B. Carpenter, R. Treece, R. Hollingsworth, G. Patel, J. Ogard, and P.K. Bhat
Materials Research Group, Inc.
Wheat Ridge, Colorado

National Renewable Energy Laboratory

1617 Cole Boulevard
Golden, Colorado 80401-3393

NREL is a U.S. Department of Energy Laboratory
Operated by Midwest Research Institute • Battelle • Bechtel

Contract No. DE-AC36-98-GO10337

September 1999 • NREL/SR-520-26382

In-Situ Sensors for Process Control of CuIn(Ga)Se_2 Module Deposition

Annual Technical Report
15 February 1998—15 February 1999

I.L. Eisgruber, T.L. Wangensteen, C. Marshall, B. Carpenter, R. Treece, R. Hollingsworth, G. Patel, J. Ogard, and P.K. Bhat
Materials Research Group, Inc.
Wheat Ridge, Colorado

NREL Technical Monitor: H.S. Ullal

Prepared under Subcontract No. ZAK-8-17619-08

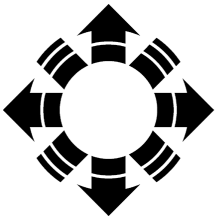

National Renewable Energy Laboratory

1617 Cole Boulevard
Golden, Colorado 80401-3393

NREL is a U.S. Department of Energy Laboratory
Operated by Midwest Research Institute • Battelle • Bechtel

Contract No. DE-AC36-98-GO10337

NOTICE

Available to DOE and DOE contractors from:
Office of Scientific and Technical Information (OSTI)
P.O. Box 62
Oak Ridge, TN 37831
Prices available by calling 423-576-8401

Available to the public from:
National Technical Information Service (NTIS)
U.S. Department of Commerce
5285 Port Royal Road
Springfield, VA 22161
703-605-6000 or 800-553-6847
or
DOE Information Bridge
http://www.doe.gov/bridge/home.html


Printed on paper containing at least 50% wastepaper, including 20% postconsumer waste

Table of Contents

List of Figures

1. Introduction

1.A Scope of the Subcontract

The use of in-situ sensors for process control is an important aspect in improving the manufacturability of thin-film $CuIn_xGa_{1-x}Se_2$ (CIGS) modules, since yield and reproducibility issues remain an important challenge in CIGS photovoltaic module fabrication. Although champion cells report impressive efficiencies, reproducing these efficiencies, particularly in large numbers, continues to be problematic[1,2]. Materials Research Group (MRG), Inc. is developing in-situ sensors to improve yield, reproducibility, average efficiency, and prevention of "lost processes". In-situ x-ray fluorescence (XRF) will be used to monitor composition and thickness of deposited layers, and in-situ optical emission spectroscopy (OES) will be used to provide real-time feedback describing the deposition plasma. Characterization techniques are to be examined ex-situ in the first two years of the contract, and applied to existing deposition systems in the final year of the contract. MRG is addressing this technology in the "R&D Partner" capacity, teamed with special services provider Lockheed Martin Astronautics (LMA).

The largest portion of the work performed in Phase I of this contract concerns development of a method to accurately deduce CIGS film thicknesses and compositions from x-ray fluorescence (XRF) signals. This method is to be developed ex-situ during the first 15 months of the contract. Important requirements for XRF analysis to be used on CIGS samples is the ability to interpret signals from multi-layer samples, to account for variations in substrate and back contact thickness, to interpret signals from samples with varying Ga gradients, and to handle samples with intermediate film thicknesses where neither thick-film nor thin-film approximations are valid. Furthermore, restrictions imposed on hardware by deposition chamber geometry, measurement time requirements during in-situ monitoring, and component costs must be considered.

1.B Introduction to X-Ray Fluorescence Measurements

X-ray fluorescence measurements are performed by illuminating a portion of the sample to be examined with x-rays and then measuring the energy and count rate of the fluoresced x-rays. Incident x-ray photons cause electrons to be ejected from atoms in the sample. As the remaining electrons fill the newly-created vacancies, thus relaxing back to the ground state, excess energy from the relaxing electrons is emitted in the form of x-rays. The energy of these fluoresced x-rays corresponds to the energy change of the electron transition, and therefore each element fluoresces at a characteristic set of x-ray energies.

X-rays resulting from the most probable transitions terminating in the K shell are referred to as "Kα" x-rays. Here "K" signifies the shell at which the transition ends, and "α" signifies that the transition started in the quantum mechanically most probable energy shell. Similarly, x-rays resulting from the most probable transitions terminating in the L shell are referred to as "Lα" x-rays. Higher energy incident x-rays are required to cause K fluorescence than to cause L fluorescence, as the electron vacancies allowing K fluorescence require more energy to create. Fluorescence occurring due to direct excitation by x-rays from the x-ray source is termed "primary fluorescence".

For in-situ monitoring, fluoresced x-ray energies and rates are measured with a solid-state energy-dispersive detector. X-rays are absorbed in the detector and create a number of electron-hole pairs, i.e. a current pulse, proportional to the x-ray energy. These pulses are amplified and then counted with a multichannel analyzer. In some XRF applications, wavelength-dispersive detection is employed. A rotating crystal is used to diffract x-rays of a given wavelength to a fixed detector. Wavelength-dispersive detection provides superior energy resolution; however, the required measurement time and the geometry of the diffraction apparatus is prohibitive for in-situ composition monitoring.

An important aspect of the XRF system configuration is the limitation of background counts. Background counts can occur because of x-rays scattered (rather than fluoresced) from the sample, x-rays fluoresced from items other than the sample, and x-rays that are absorbed in inactive areas of the detector. Background can be minimized in a number of manners. The solid angle of the x-rays reaching the detector should be limited through collimation, so that the detector is exposed only to x-rays from the illuminated portion of the sample. An appropriate backing material should be placed behind the sample to absorb transmitted x-rays. Use of a monoenergetic x-ray source can decrease background counts in an energy region of interest that is far-removed from the incident x-ray energy, since each scattering event causes only a small energy shift in the scattered photon.

2. Simulation Tool For XRF Signals

2.A The Importance of Simulating XRF Signals

MRG has developed a tool that simulates the XRF of multilayer structures. This tool is used to troubleshoot measurements, to predict difficulties in XRF interpretation, and to calculate quantities needed in the translation from XRF signal to composition. Each of these uses for the simulation tool is discussed in the following paragraphs.

A simulation tool is important for troubleshooting XRF measurements. A number of artifacts - such as those due to x-ray tube intensity drift, scattering of x-rays to surrounding materials, signals from elements in the sample substrate, signal from x-rays transmitted through the sample, or sample non-uniformity - may appear in measurements. The simulation tool allows comparison of measured signals on known samples with calculated signals. Artifacts encountered to date in XRF measurements at LMA are discussed in the section "4. XRF measurements".

The simulation tool is also useful for predicting difficulties in XRF interpretation. Quantitative interpretation of XRF signals can be complicated, since interactions occur between the signal from one element and the other elements in the sample. These interactions may occur as absorption of incident and fluoresced x-rays by the other elements in the sample, or by excitation of the given element by x-rays fluoresced from the other elements ("secondary fluorescence"). For example, increasing the amount of Ga / (In + Ga) ratio of a CIGS sample will increase the signal from the Cu, since Cu is efficiently excited by Ga fluorescence, and Ga absorbs Cu emission less efficiently than In. Similarly, variations in the Mo back contact thickness will cause variations in the secondary fluorescence emission of Cu, Ga, and Se in the sample. The simulation tool can calculate the expected XRF signal from such samples and therefore define the expected strengths and limitations of the sensing technique. The implications of various simulations for extracting composition are discussed in the section "2.D Implications of XRF Simulations for In-Situ Sensing of CIGS".

Finally, the simulation tool can calculate the quantities needed to translate XRF signal to composition. Such capability is needed because the first principles equations that calculate XRF signal from a known sample cannot be inverted to extract layer compositions from XRF signals of an unknown sample. Thus, a number of numerical methods exist for extracting sample composition from XRF signals[3,4,5,6,7,8,9,10]. Important requirements for such a method to be used on CIGS samples are the ability to interpret signals from multi-layer samples, to account for variations in substrate and back contact thickness, to interpret signals from samples with varying Ga gradients, and to handle samples with intermediate film thicknesses where neither thick-film or thin-film approximations are valid. The approach to be taken is similar to that used by de Jongh for analysis of stainless steels[10]. The relationship between the composition of the sample and the XRF counts is expressed as a first-order Taylor expansion, and the coefficients in the Taylor expansion are calculated numerically from first principles using the simulation tool. These relationships can then be algebraically inverted to extract the parameters describing the physical make-up of the CIGS sample.

2.B Development of Theoretical Foundation for Simulation Tool

The equations that predict magnitude of x-ray fluorescence signals from a homogeneous, single-layer sample are well known, although complicated[11]. This analysis was extended to multi-layer samples at MRG, to find the from a multi-layer sample. It was deduced that the photons per area, per solid angle, detected from the fluorescence of element i in layer k is

$$P_{i,k} = q\ E_{i,k}\ C_{i,k}\ e^{-\frac{1}{\sin\Psi_2}\sum_{\ell=1}^{k-1}\mu_{s\ell}(\lambda_{i,k})\rho_\ell h_\ell} \bullet \int_{\lambda_o}^{\lambda_{abs,i,k}} \left\{1 - e^{-\rho_k h_k\left(\frac{\mu_{sk}(\lambda)}{\sin\psi_1} + \frac{\mu_{sk}(\lambda_{i,k})}{\sin\psi_2}\right)}\right\} \bullet e^{-\frac{1}{\sin\psi_1}\left[\sum_{\ell=1}^{k-1}\mu_{s\ell}(\lambda)\rho_\ell h_\ell\right]} \frac{\mu_{ik}(\lambda) I_\circ(\lambda)\, d\lambda}{\mu_{sk}(\lambda) + \frac{\sin\psi_1}{\sin\psi_2}\mu_{s,k}(\lambda_{i,k})} \qquad (1)$$

where

$P_{i,k}$ = the photons per second per area of illuminated sample fluoresced into the specified solid angle

k = index specifying which layer in the sample

i = index specifying which element within layer k

ℓ = index used for sums over multiple layers

Ψ_1 = the angle between the incident x-ray beam and the sample surface

Ψ_2 = the angle between the sample surface and the path from the illuminated spot to the detector

q = the geometric factor $\frac{\sin\psi_1}{\sin\psi_2}\frac{d\Omega}{4\pi}$, where $d\Omega$ is the solid angle subtended by the detector, relative to the sample

$E_{i,k}$ = the excitation factor, which involves the quantum mechanical probability of the photons of interest being produced and escaping the atom

$C_{i,k}$ = the concentration by weight of element i in layer k

$\lambda_{abs,\,i,\,k}$ = absorption edge wavelength of element i in layer k

λ_0 = the highest energy wavelength present in the incident x-rays

λ = the variable used to integrate over all the wavelength range of the incident x-rays

$\lambda_{i,k}$ = the fluorescence wavelength of element i in layer k

$\mu_{s\ell}$ = the mass absorption coefficient of the layer ℓ

μ_{sk} = the mass absorption coefficient of the layer k

μ_{ik} = the mass absorption coefficient of element i in layer k

ρ_ℓ = the density of layer ℓ
ρ_k = the density of layer k
h_ℓ = the thickness of layer ℓ
h_k = the thickness of layer k
I_0 = number of incident photons per second per area at a given wavelength

The secondary fluorescence, i.e. fluorescence excited not from the incident x-rays but from a constituent element's fluorescence, can also be calculated. For a multi-layer sample, such an expression was derived at MRG. It was found that the number of photons per solid angle detected due to the secondary fluorescence of element i in layer k excited by element j in layer $\square$ is

$$S_{i,j,k,\ell} = \frac{1}{2} q E_i C_{ik} E_j C_{j\ell} \frac{\rho_k \rho_\ell}{\sin\psi_1} \mu_i(\lambda_j) \int_{x_\ell=0}^{t_\ell} \int_{y_k=0}^{t_k} U'(x_\ell, y_k)\, A'(x_\ell)\, B'(y_k)\, dx\, dy \qquad (2)$$

where

$$U'(x, y) = \int_{\alpha=0}^{90^\circ} \tan(\alpha)\ \xi\ d\alpha$$

$$A'(x_\ell) = \int_{\lambda_{\min}}^{\lambda_{abs,j}} \mu_j(\lambda_{inc})\, I_\lambda\, A_1 \exp\left[\frac{-1}{\sin\psi_1}\left(\mu_{s\ell}(\lambda_{inc})\rho_\ell x_\ell + \sum_{p=1}^{\ell-1} \mu_{sp}(\lambda_{inc})\rho_p t_p\right)\right] d\lambda_{inc}$$

$$B'(y_k) = \exp\left[-\mu_{sk}(\lambda_i)\rho_k \frac{y_k}{\sin\Psi_2} - \sum_{p=1}^{k-1} \mu_{sp}(\lambda_i)\rho_p \frac{t_p}{\sin\psi_2}\right]$$

$$\xi = \begin{cases} \exp\left[-\mu_k(\lambda_j)\rho_k \dfrac{|x-y|}{\cos\alpha}\right] & (\ell = k) \\ \exp\left[-\sum_m \mu_m(\lambda_j)\rho_m \dfrac{t_m}{\cos\alpha} - \mu_\ell(\lambda_j)\rho_\ell \dfrac{x_\ell}{\cos\alpha} - \mu_k(\lambda_j)\rho_k \dfrac{(t_k - y)}{\cos\alpha}\right] & (\ell > k) \\ \exp\left[-\sum_m \mu_m(\lambda_j)\rho_m \dfrac{t_m}{\cos\alpha} - \mu_\ell(\lambda_j)\rho_\ell \dfrac{(t_\ell - x)}{\cos\alpha} - \mu_k(\lambda_j)\rho_k \dfrac{y}{\cos\alpha}\right] & (\ell < k) \end{cases}$$

α = Variable of integration in U'(x,y)
A_1=incident beam area
and other variables are as defined in equation (1).

The integrals in equations (1) and (2) are calculated numerically. Algorithms are included to insure that the error introduced by the finite step size in the numerical integration stays below the specified maximum percent error. Incident spectra and fundamental constants such as densities and mass absorption coefficients, and are taken from the literature[12]. The simulation tool outputs the magnitude of primary and secondary fluorescence emission lines from multi-layer samples, where each layer contains multiple elements.

Emission from both K and L transitions is calculated. Sample output from the simulation tool is shown in Figure 1.

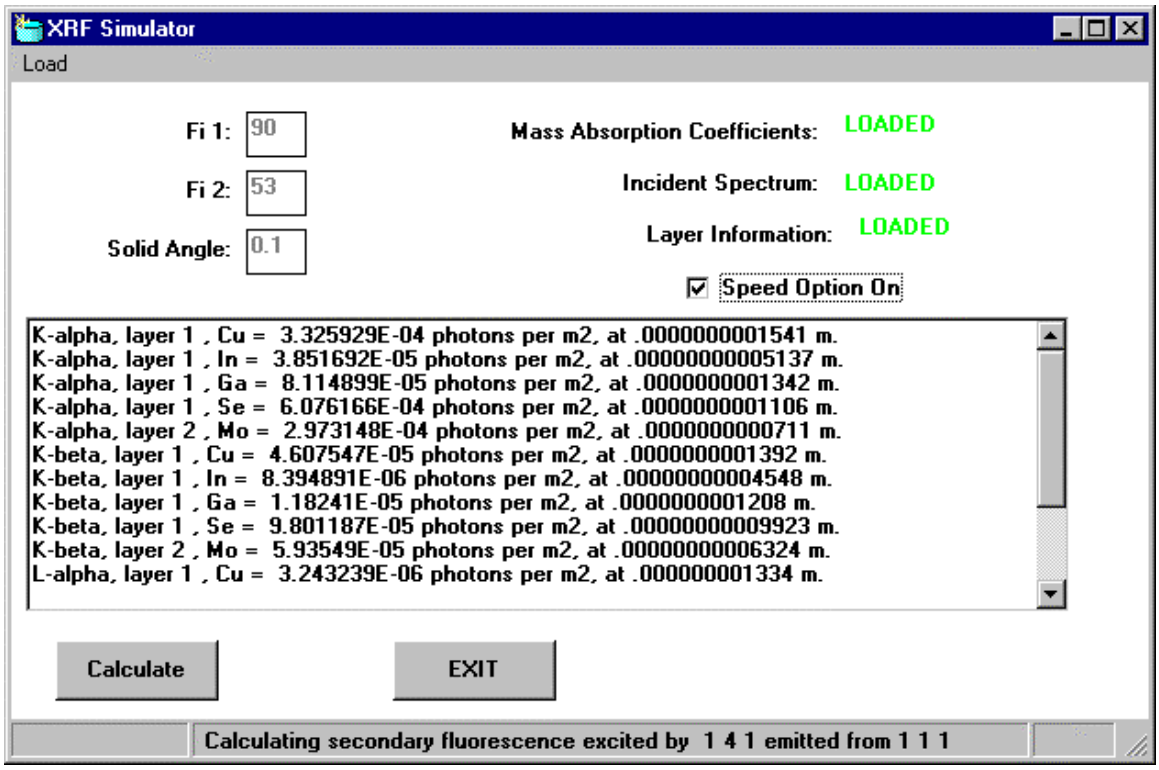

Figure 1: Sample output from XRF simulation tool.

2.C Verification of Correct Results of Simulation Tool

A number of tests have been performed to verify the simulation output. Comparisons of the simulator output both with simplified theoretical expressions and with published data have been made. This section describes the verifications of the simulator output.

For very thick and very thin films, equation (1) can be simplified considerably[13]. In such cases, for monochromatic incident x-rays, the integral in equation (1) can be performed, and algebraic expressions for the primary fluorescence can then be written. Figure 2 shows the simplified theoretical expressions for the fluorescence from thick and thin Cu films, shown as the solid and dotted lines, respectively. The simulator output is also shown, and agrees with the theoretical expressions over the appropriate thickness ranges. As expected, for very thick films the count rate is independent of the film thickness. The count rates shown on the y-axis are for a specified system geometry and incident x-ray flux, and therefore should not be taken as a general indicator of count rates.

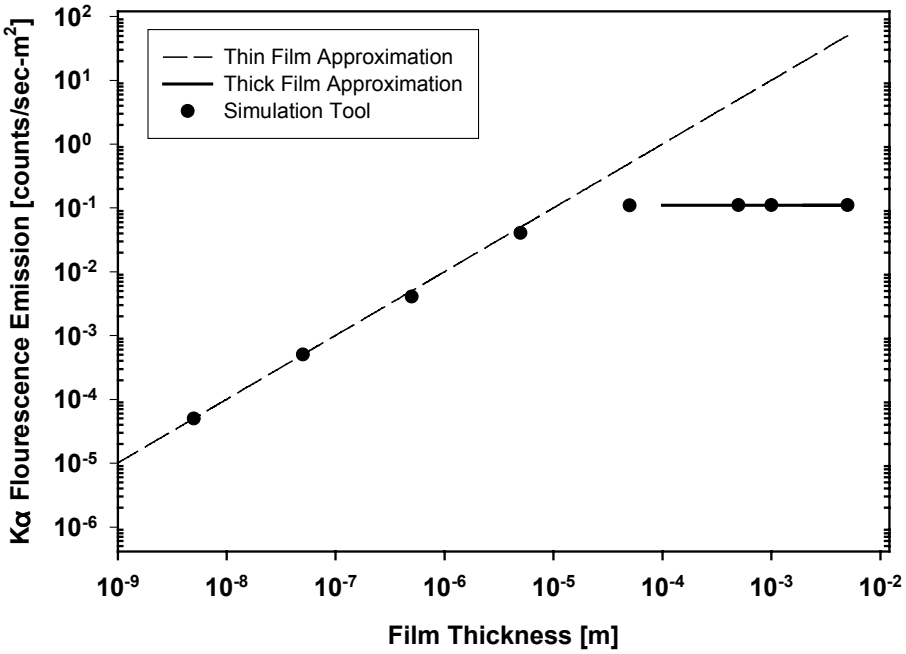

Figure 2: Comparison of simulator output with theoretical expressions for Kα primary fluorescence of thick and thin Cu films.

Similarly, a simplified expression for the secondary fluorescence of thick films can also be obtained[14]. Simulator output was shown to agree with the simplified theoretical expression for secondary fluorescence as well.

Simulation output was tested against published XRF data. For example, Bush and Stebel[15] measured the XRF of Ag films of varying thickness on Cu substrates. The change in Ag signal and Cu signal they measured is plotted in Figure 3 as the filled points. The output of the XRF simulator is shown as the open points, and agrees well with the measured data.

Simulation output for secondary fluorescence was also tested against published XRF data. For example, Pollai et al.[16] calculated the ratio of secondary to primary fluorescence intensity as a function of film thickness for Cu-Co alloys. MRG simulator output was compared with the published data, as shown in Figure 4. The filled circles show Pollai's data. The open squares show the simulator output, which agrees well with Pollai's data. It should be noted that the ratio of secondary to primary fluorescence depends strongly on the incident x-ray spectrum. The gray triangles show the simulator output when Rh characteristic radiation is used as the incident spectrum, rather than the typical Rh tube spectrum that includes continuous as well as characteristic radiation. The exact incident spectrum used by Pollai et al. is not available.

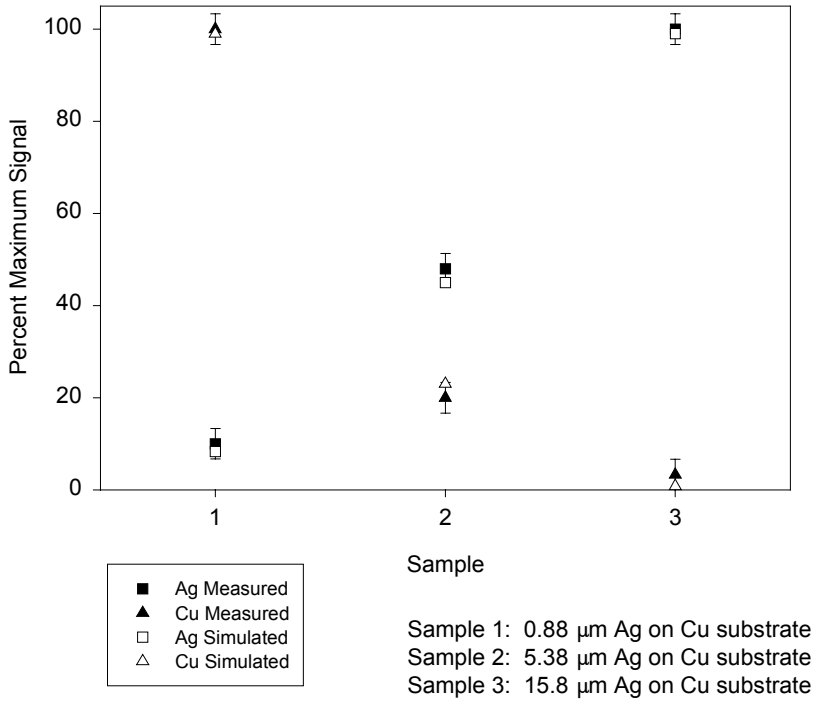

Figure 3: Measured and calculated change in Ag and Cu XRF signals for Ag layers of varying thicknesses on Cu substrates.

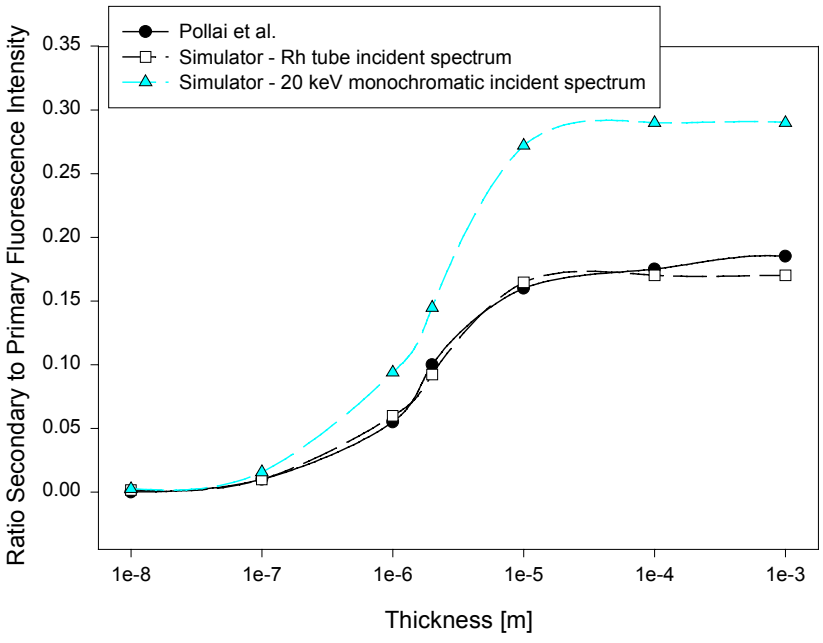

Figure 4: Ratio of secondary to primary fluorescence intensity versus film thickness for 50% Cu - 50% Co alloys.

Finally, a number of tests were performed to insure that simulator output is self-consistent. These tests included verifying that the same output is obtained i) in the case of a sample layer that is 100% element A and in the case where the sample layer contains 50% element A and 50% element B, and element B has properties identical to element A; ii) regardless of the order of listing elements within a layer; and iii) in the case where a sample is made of 1 layer of element A and in the case where the sample is made of multiple layers of element A having the same total thickness as in the first case. It was also verified that small changes in the input concentrations and material properties produced changes in the output that were smooth and qualitatively correct.

2.D Implications of XRF Simulations for In-Situ Sensing of CIGS

Qualitative interpretation of XRF signals is simple: the more of a given element is present, the stronger is that element's fluorescence. Quantitative interpretation, however, becomes more complicated, since interactions occur between the signal from one element and the other elements in the sample. These interactions occur in two manners: (i) absorption of incident and fluoresced x-rays by the other elements, and (ii) excitation of the given element by x-rays fluoresced from the other elements ("secondary fluorescence"). The simulation tool developed at MRG can be used to for predict the presence and severity of such interactions in XRF interpretation.

For example, Figure 5 shows the calculated effect of varying Ga content on XRF signal. Calculations were performed for a uniform 2.5 μm CIGS film illuminated by 20 keV x-rays, the characteristic radiation from a Rh anode. Varying Ga/(In + Ga) ratio is plotted on the x-axis. On the y-axis, the fraction of emission for each peak, relative to that from a sample with Ga/(In + Ga) = 0.25, is plotted. As expected, Ga signal increases and In signal decreases nearly linearly with Ga addition.

Figure 5b is a magnification of the data shown in Figure 5a, emphasizing the effects of interaction between elements. Over the range of Ga concentrations shown, the Cu signal increases by 6% even though the number of Cu atoms in the sample is constant. This increase occurs for two reasons. First, the mass absorption coefficient of In (in m^2/mole) is about 6 times greater than that of Ga at the Cu emission wavelength. Thus, increasing replacing In atoms with Ga atoms allows more Cu fluorescence to escape the sample. Second, Cu fluorescence is excited very efficiently by Ga-Kα emission, so as the amount of Ga increases, Cu emission from secondary fluorescence also increases. The Se signal, on the other hand, shows very little change with the addition of Ga, because the mass absorption coefficients of Ga and In are nearly equal at both the incident and the Se emission wavelength. Furthermore, the Se absorption

edge is at a higher energy than the Ga emission, so no secondary fluorescence signal enhancement occurs.

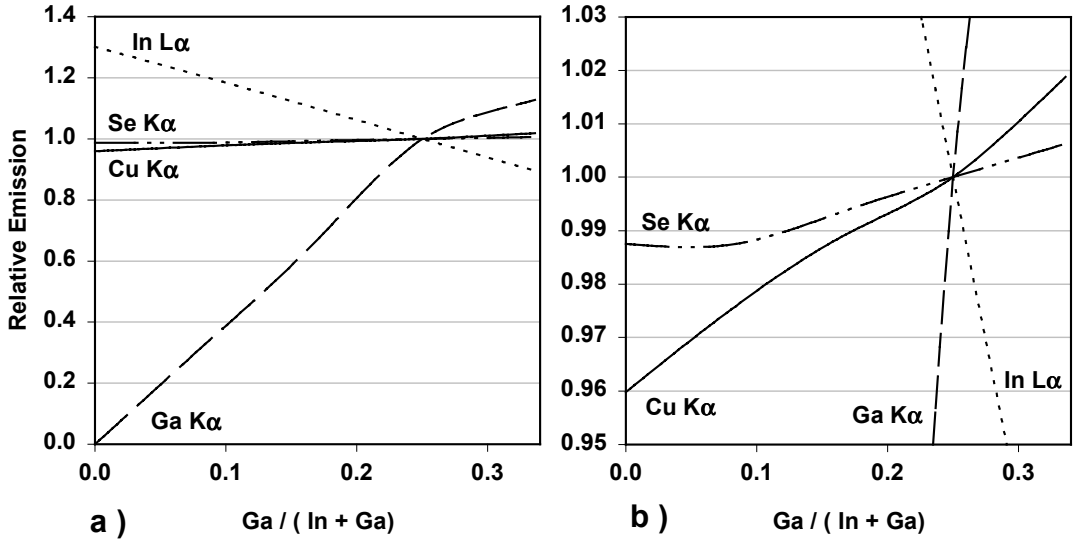

Figure 5: Calculated effect of varying Ga content on XRF Cu-Kα, In-Lα, Ga-Kα, and Se-Kα signals, for a uniform 2.5 μm CIGS film illuminated by 20 keV x-rays.

Variations in back contact thickness may have an effect on fluorescence signals similar to that seen in Figure 5. A thicker back contact means more intense Mo Kα emissions are available for exciting secondary fluorescence in the CIGS. Furthermore, depending on the thickness of the back contact, fluorescence from elements contained in the substrate may or may not be present in the measured signals.

Through-film concentration gradients can also cause complications in the interpretation of XRF data. If a given element is concentrated at the front of a sample, it will yield a higher XRF signal than another sample containing the same amount of the element concentrated at the back of the film. Figure 6 shows calculated effect of Ga gradient on XRF signal. Once again, calculations were performed for a 2.5 μm CIGS film illuminated by 20 keV x-rays. All data in Figure 6 is for films containing the same number of Ga atoms, but the gradient in the Ga/(In + Ga) ratio, R, is plotted on the x-axis. A film with dR/dt = 0 corresponds to a uniform film with Ga/(In + Ga) = 0.25. A film with dR/dt = -0.2 corresponds to the case where Ga/(In + Ga) changes by –0.2 every micron, so Ga/(In + Ga) = 0.5 at the front of the film and 0 at the back of the film. Even though the numbers

of In atoms and Ga atoms in the film are constant across the graph, the In and Ga signals depend on the locations of these atoms within the film.

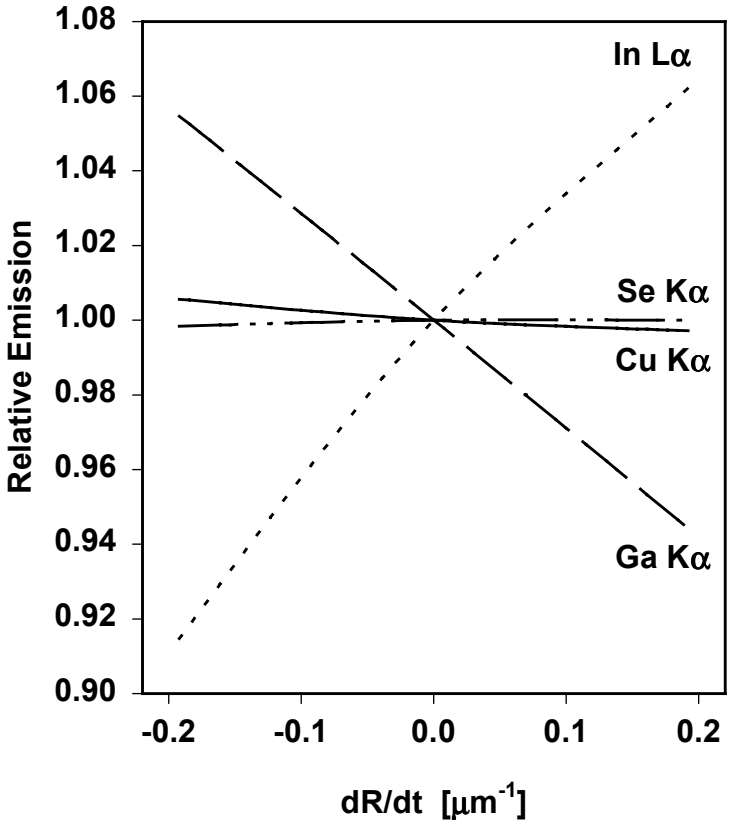

Figure 6: Calculated effect of gradient in the ratio R, defined as Ga/(In + Ga), on XRF signals from 2.5 μm CIGS films containing the same total number of Ga atoms.

Substrate impurities can be an important factor in the interpretation of XRF data as well. It is calculated, for example, that the Cu signal from a typical CIS/Mo/glass sample will be increased by 3.7% if the glass contains Cu impurities of only 0.1% by weight. Thus, each type of substrate must be evaluated for its effect on XRF analysis.

3. Sample Fabrication

A number of samples were fabricated for XRF measurements. These samples include single-element, layered, CIS, and CIGS samples. Samples were made at LMA on 12" x 12" glass, using the Dynamic Research System at LMA[17]. Many samples were intentionally graded by changing the transport speed as the substrate passed over the sputtering target(s). The purpose of the fabricated samples is three-fold. First, multi-layer samples and samples of

varying thickness are used to verify the expected dependencies of XRF signal on sample geometry, thereby allowing identification and removal of measurement artifacts. Second, single-element samples of a known thickness are used to calibrate the XRF signal to the amount of analyte present. Third, samples of known gradients in composition are used to compare various methods of measuring composition to be used later in verifying XRF analysis of unknown samples.

A simple method for determining the transport speeds and time intervals necessary to create a desired sample grading was developed. The minimum and maximum thicknesses are subject to limits imposed by the sample size, transport speeds, and deposition rates.

The method for fabricating graded samples was verified experimentally. Figure 7 shows the measured and intended thickness as a function of position on a graded 12" x 12" Cu sample. (Uniformity perpendicular to the direction of the grading is better than ±2%.) Vertical error bars on the measured points represent the uncertainty in the mechanical profilometer measurements. The small percentage disagreement seen between the measured and the intended thicknesses is largely due to uncertainty in the transport speed.

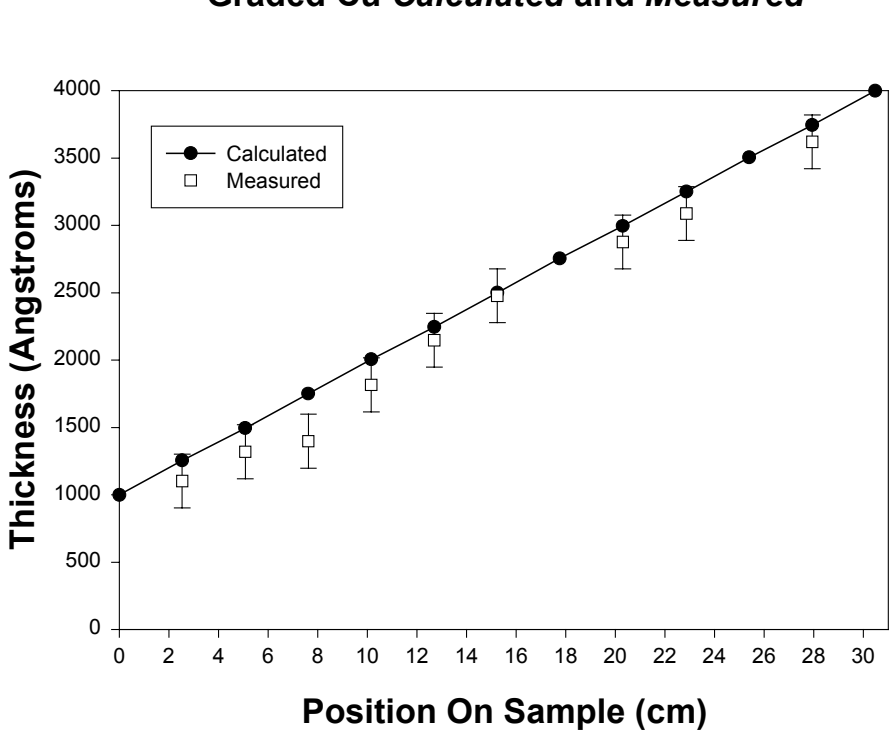

Figure 7: Measured and calculated thickness of a graded Cu sample.

Table 1 lists samples fabricated at LMA. for XRF analysis. All thickness gradients occur across the 14" sample length.

Sample Number	Structure	Cu Thickness	In Thickness	Ga Thickness	Comments
LMA01099A	Glass/Cu	1 μm	--	--	--
LMA06199B	Glass/Mo	--	--	--	--
LMA04138A	Glass/Mo/CIS	2496 Å	4230 Å	--	Stoichiometric CIS
LMA04179A	Glass/Mo/CIS	Graded 1000 to 4000 Å	4230 Å	--	Graded from stoichiometric to (Cu+)
LMA09049B	Glass/Mo/Cu	Graded 1000 to 4000 Å	--	--	--
LMA0598A	Glass/Mo/Cu/In	Graded 1000 to 4000 Å	Graded 4000 to 10000 Å	--	Cu gradient at 90° to In gradient
LMA04289B	Glass/Mo/CIS	Graded 1400 to 2600 Å	4230 Å	--	Graded from stoichiometric to (Cu-)
LMA05299A	Glass/Mo/CIGS	2496 Å	4094 Å	Graded 1000 to 1700 Å	Graded from Ga/In+Ga= 0.2 to 0.3
LMA04039C	Polyimide/Mo/ CIGS	2496 Å	4094 Å	1350 Å	--

Table 1: Samples fabricated at LMA for XRF analysis.

Preliminary comparisons of composition measurement techniques were made on samples containing known elemental gradients. A CIS sample was fabricated with uniform In thickness and Se exposure, but graded Cu thickness across the 12" sample length. Three pieces were cut from this sample and analyzed at the National Renewable Energy Laboratory for composition by electron probe microanalysis (EMPA) and inductively coupled plasma (ICP). Table 2 shows the obtained data. Note that the effective layer thickness derived from ICP depends on the accuracy with which the sample area is cut and also the accuracy with which volume of the acidic solution is measured. Samples for which data is shown measured 2.54 ± 0.1 cm per side, implying an uncertainty in area of ±8%. A ±5% uncertainty in the solution volume implies that close to a ±15% systematic error may exist in each sample's ICP effective thicknesses.

Position along graded sample:	1.5"			4.5"			10.5"		
	Cu	In	Se	Cu	In	Se	Cu	In	Se
ICP atomic %	32.2	21.6	46.2	33.4	20.8	45.8	35.0	19.3	45.7
ICP effective thickness (Å)	2609	3881	8651	3196	4415	10107	3240	3944	9771
EPMA atomic %	30.8	21.6	47.6	32.3	20.8	46.8	25.3	24.9	49.8
Thickness Deposited	2119	4230		2355	4230		2847	4230	

Table 2: Comparison of composition information deduced from ICP measurements, EPMA measurements, and deposition conditions.

Sample Cu thicknesses, as derived from ICP measurements and from deposition conditions, are shown in Figure 8. In this figure, error from sample area measurements, as mentioned in the paragraph above, was removed by assuming that the In thickness for each sample was 4230 Å, as calculated from the uniform In depositions. The amount of Cu detected in ICP measurements shows roughly the same percentage change as that expected from deposition conditions. Some disagreement, most likely due to uncertainty in transport speed and to ICP measurement calibration, is apparent.

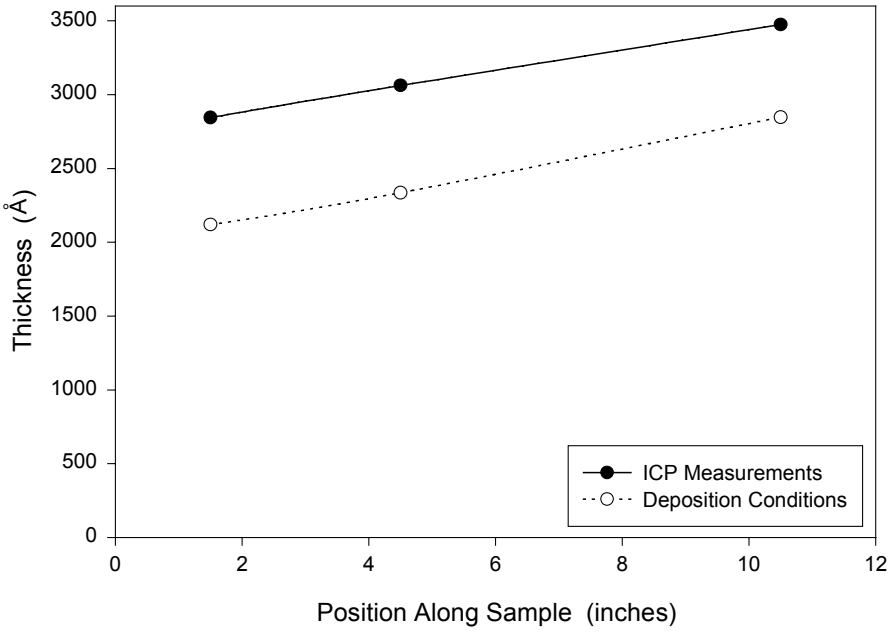

Figure 8: Sample Cu thicknesses, as determined by deposition conditions and ICP measurements.

The comparison shown in Figure 8, Cu thickness measured by different techniques, is actually a better variable of comparison than atomic percent for off-stoichiometry samples. Thickness is a more direct comparison, since the incorporation of Se into the sample is controlled not by the exposure of the sample to Se, but actually by the composition of the growing film[26]. Thus, comparisons of atomic percent reflect not only the change in Cu in the sample, but also the change in Se incorporation. For example, in Table 2, normalizing all In thicknesses to 4230 Å to correct for differences in sample area, the thickness of Se present in the samples increases from 9429 Å, to 9683 Å, to 10479 Å, as the Cu increases in the sample. Such increases are consistent with the formation of Cu_xSe_y phases including more than one Se atom per Cu atom.

Figure 9 shows atomic percent composition data as measured by ICP and by EPMA on the same graded samples as discussed above. Error bars on EPMA measurements represent statistical, not systematic, errors. The EPMA

measurements show consistently more Se and less Cu than the ICP measurements. This difference may be due to the penetration depth of the measurements. ICP tests the entire sample uniformly, whereas the EPMA sampling depths are typically around 1 μm[18]. An EPMA sampling depth less than the 2.5 μm CIS thickness is confirmed by lack of Mo signal in the measurements. In contrast, during XRF measurements, a Cu sample must be about 12 μm thick to absorb just 50% of the 20 keV incident x-rays.

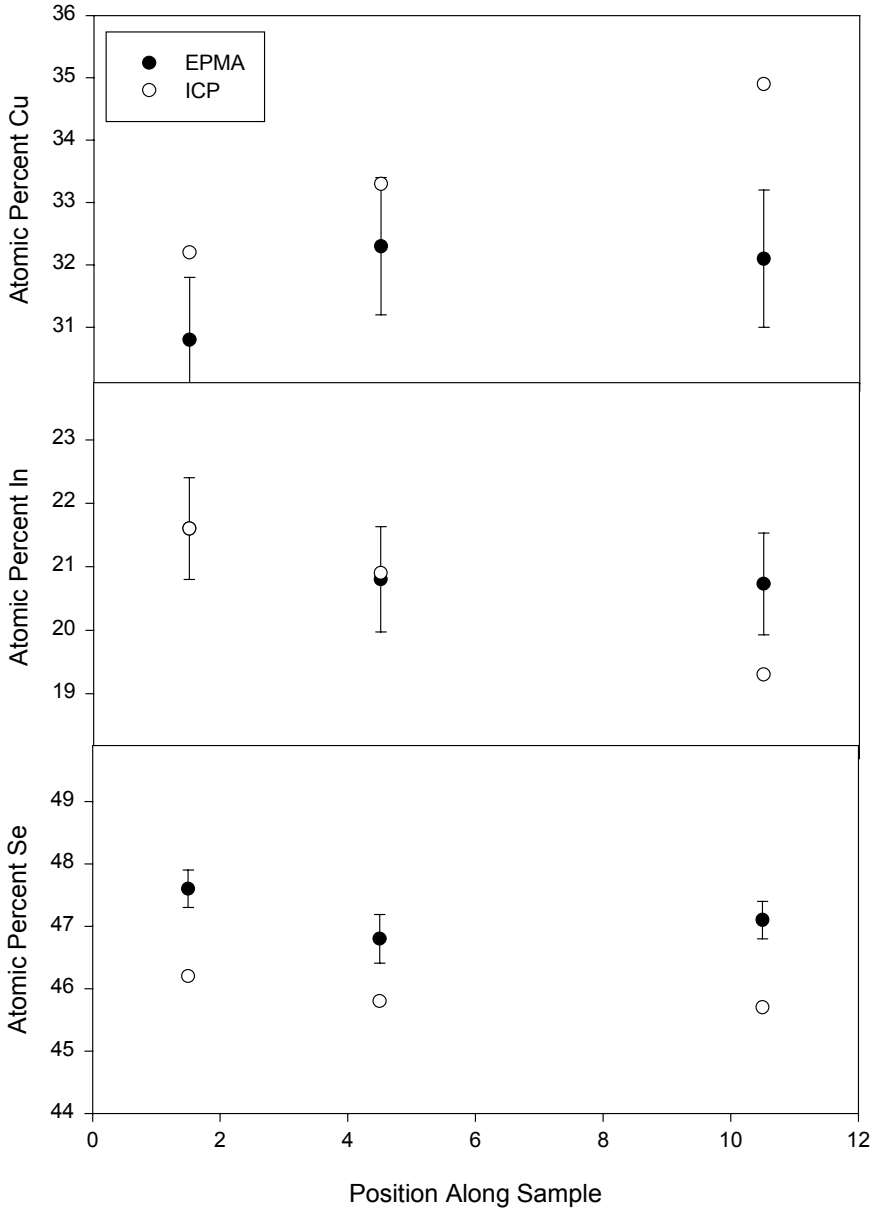

Figure 9: Comparison of atomic percent composition as measured by ICP and EPMA.

In conclusion, the comparison of deposition conditions, ICP measurements, and EPMA measurements suggests that ICP measurements may be a more suitable check on XRF measurements than EPMA measurements, for several reasons. First, ICP measurements accurately reflect the percent change in the amount of Cu predicted from deposition conditions. Second, EPMA measurements do not clearly reflect the expected change in Cu. Third, EPMA measurements appear to be assessing the front portion of the sample, whereas ICP measurements assess the entire sample uniformly. The whole-sample assessment is most representative of the absorption of incident x-rays during XRF measurements.

4. XRF measurements

XRF measurements were made at LMA. The LMA system consists of a 30 keV, 3 mA, Rh x-ray tube, a collimator, a LN-cooled Si(Li) detector, and detection electronics

High purity Nb foil was used as a backing material during XRF measurements. Backing material is necessary because the XRF samples are thin. For thin samples, a significant fraction of the incident x-rays are transmitted through the film and will cause fluorescence in areas behind the film. Thus, a backing material, such as Nb foil, that does not contain any x-ray emission lines overlapping with those of Cu, In, Ga, and Se, must be located behind the illuminated portion of the sample. A further requirement for the backing material is that for future uses it be compatible with a Se-containing environment, eliminating hydrogen displacing metals such as Al, Zn, Fe, Na, Ca, and soft steels. Figure 10 shows the location in energy of emission lines from Cu, In, Ga, Se, and Mo, as well as from the potential backing materials Nb and Ti. Nb is the less expensive choice. Emission lines in Figure 10 are shown with a 250 keV full width at half maximum.

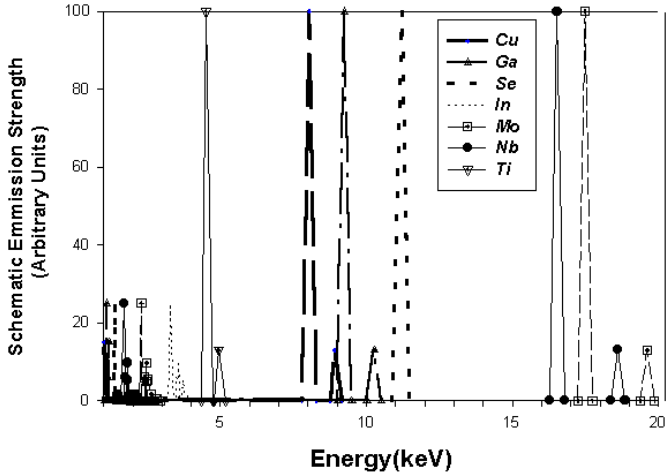

Figure 10: X-ray fluorescence lines expected to be seen in CIGS samples, as well as those from potential backing materials Nb and Ti.

Measurement reproducibility was verified. The minimum relative standard deviation in the number of counts, N, in a fluorescent peak is dictated by the statistics of independent events and is therefore $\frac{\sqrt{N}}{N}$. For example, the number of Mo counts from the same position on a sample was measured repeatedly. The average number of counts was $\overline{N}$ = 276,716. The relative standard deviation of the measurements about the mean was 0.35% ± 0.20%, where the uncertainty interval was determined by 95% confidence intervals. The standard deviation to be statistically expected is 0.19%, which is within the above range.

A number of issues were resolved regarding the proprietary Kevex® analysis routines that are automatically performed on the XRF spectra by the data acquisition equipment. The method used for peak deconvolution was determined, and a means of obtaining numerical output of the raw data was obtained. This raw numerical output can be used for analysis not possible with the Kevex® routines, for graphing, and possibly in the future for use with closed-loop control.

XRF measurements on glass/Mo/Cu samples were made to verify the expected dependency of Mo and Cu signals on Cu thickness. Such verification is necessary to identify and interpret any artifacts in the measurement. To unexpected effects were observed. First, Mo signal was extremely nonuniform with position. Second, the Cu signal, although it followed the correct qualitative trend, did not quantitatively follow the expected relationship with Cu thickness. Each of these effects is discussed in more detail below.

Figure 11 shows the measured versus expected relative change in Mo thickness as a function of position, on a glass/Mo/graded Cu sample. The expected signal was calculated using the MRG simulation tool, and the Cu thickness on the x-axis was measured by mechanical profilometer. Calculated points are shown as cross-hairs, and measured points are the solid circles. The magnitude of the calculated points was normalized to the first measured point, to account for unknown geometric factors and x-ray tube flux. The Mo was deposited in LMA's C-Mag® system utilizing a 3" diameter x 16" long cylindrical magnetron sputtering target. For a uniform Mo layer, the Mo signal should decrease very slightly (~2%) with Cu thickness, as more of the fluoresced Mo emission is absorbed in the Cu. Instead, the Mo signal fluctuates by 155%, in no recognizable pattern, across the sample.

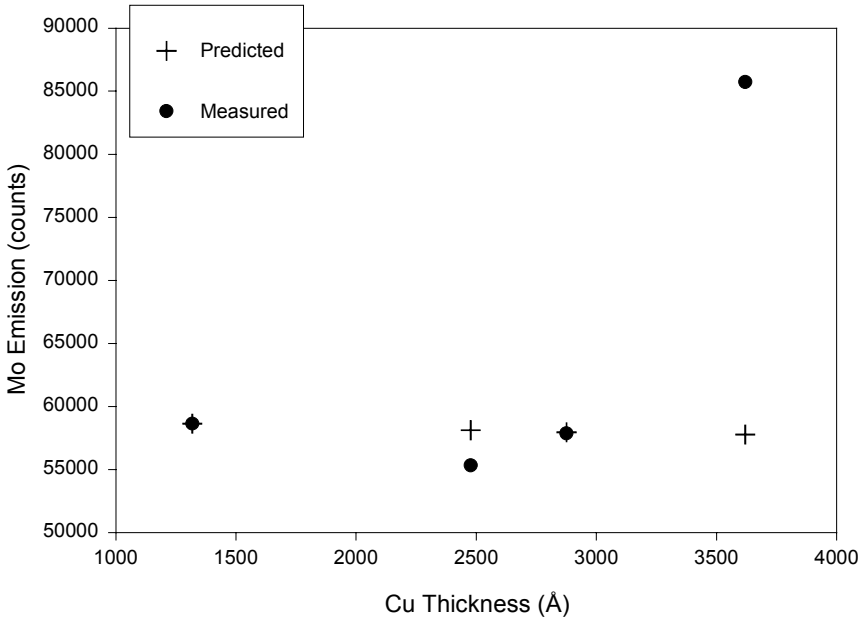

Figure 11: Measured and expected change in Mo XRF signal as a function of position on a glass/Mo/graded Cu sample.

To examine the source of the nonuniform Mo signals, a partially masked 14" x 14" Mo sample was fabricated. Thickness was measured at 27 random points along the sample. Measured thicknesses varied from 9500 Å to 14200 Å. The thickness variations showed no pattern, indicating a rough, rather than graded, sample. The 150% measured thickness variation can account for the observed XRF fluctuations.

The thickness variations in the Mo have several implications for XRF measurements on CIGS. First, for samples with rough Mo, the attenuation of the XRF signal from the Mo cannot be used as a gauge of the CIGS thickness. Likewise, the XRF Mo signal cannot be used to correct for changes in x-ray tube intensity. Finally, a varying Mo signal will cause the signals from the elements in the CIGS to change slightly, due to secondary fluorescence effects. It is calculated, for example, that the observed variations in Mo thickness will cause a 0.5% variation in the Cu signal due to changes in secondary fluorescence.

The second unexpected result uncovered during the measurement of the graded Cu/Mo/glass samples was that the Cu signal did not follow the expected quantitative relationship with Cu thickness. Figure 12 shows measured and expected Cu emission as a function of position on the graded sample. The filled points show the measured data, and the open points show the expected data.

The magnitude of the calculated points was normalized to the largest measured point, to account for unknown geometric factors and x-ray tube flux. The error bars in the x-direction represent uncertainty in the mechanical profilometer measurements. Although the Cu emission follows the correct qualitative trend, increasing with Cu thickness, quantitative agreement is not good.

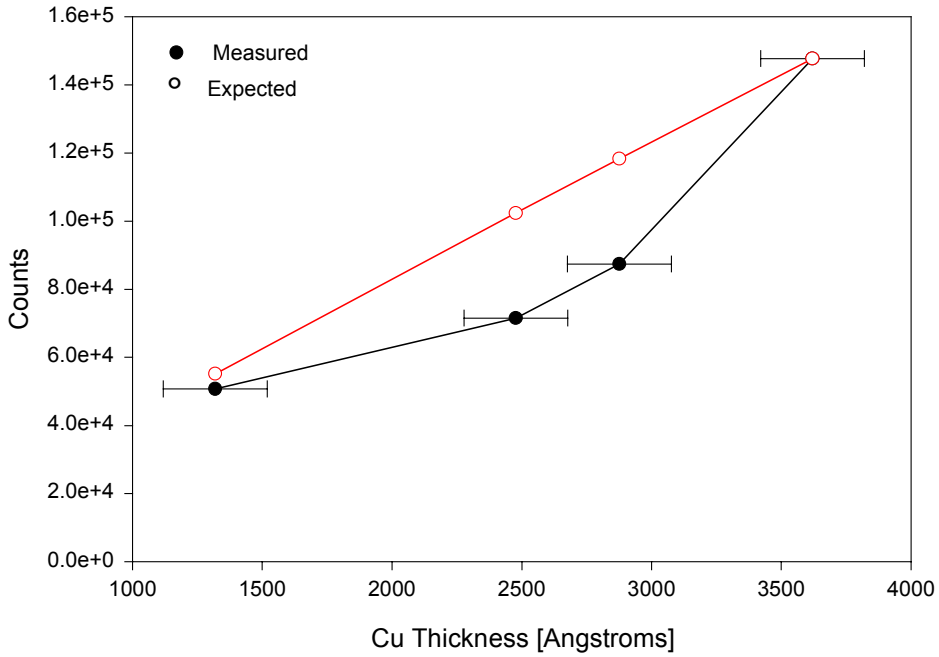

Figure 12: Measured and expected Cu signal as a function of position on graded Cu/Mo/glass sample.

Cu contamination of the XRF equipment was found to be a contributing factor in the unexpected quantitative behavior of the Cu signal. Figure 13 shows a fluorescent spectrum measured with the Nb backing material alone in the test position. A distinct Cu peak, at 8.04 keV, is seen. Table 3 lists the Cu counts and Nb counts as a function of position on the foil. The Cu counts range from 1.5% to 3.1% of the Nb counts. The Nb foil is specified at 127 μm thick and 99.8% pure, implying that if all impurities in the Nb were Cu, and the Nb foil was placed on a pure Cu substrate, the Cu should yield only 0.17% the number of counts as the Nb. (This result was calculated using the MRG simulation tool.) Upon dismantling the x-ray tube, a copper-colored film was observed coating parts on the tube. After etching the x-ray tube and sandblasting the collimator, the Cu and Nb counts were listed as in Table 4. Note that although the number of Cu counts relative to the number of Nb counts was reduced by the etch and sandblast, the Cu counts were not eliminated. Investigations into the source of the remaining Cu contamination are ongoing. After elimination of Cu contamination, substrate effects will also be examined as a source of the quantitative disagreement between expected and measured Cu emission.

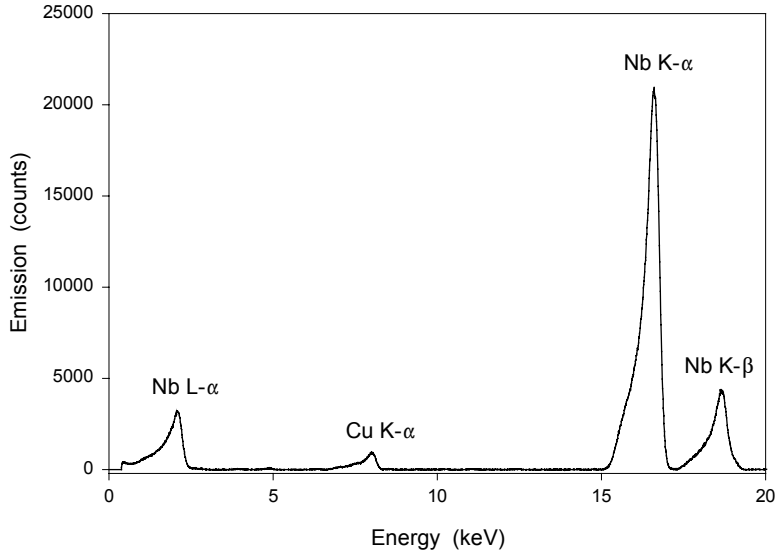

Figure 13: Measured fluorescence spectrum of high purity Nb foil.

Position Number	Nb Counts	Cu Counts	Cu/Nb Ratio
70	430710	13500	3.13%
86	303680	6341	2.09%
87	414066	6410	1.55%

Table 3: Measured Cu and Nb counts as a function of position on Nb foil.

Position Number	Nb Counts	Cu Counts	Cu/Nb Ratio
70	580907	17869	3.08%
86	563114	4931	0.88%
87	587575	4976	0.85%

Table 4: Measured Cu and Nb counts as a function of position on Nb foil after etching x-ray tube and sandblasting collimator.

5. In-situ XRF Sensor Design

Hardware for an in-situ XRF sensor, built entirely of commercially available and cost-effect components, was designed. Leading to the design of this sensor, a number of issues impacting the sensor specifications were examined. Those issues, as well as the sensor design, are discussed below.

First, a survey of existing, commercially available, complete XRF systems was performed. Such systems were found to exist in roughly four varieties: (i) portable units for soil and metals analysis, (ii) desktop units, (iii) integrated

"process control units", and (iv) completely unintegrated components. Many of these available units do have the required sensitivity for measurement of CIGS thin films. However, they are not vacuum-compatible, require very small (1 mm to 1 cm) detector-to-sample distances, and are not fitted with the analysis and outputs necessary for CIGS closed-loop process control. Portable units are priced in the $40,000 to $60,000 range. They use a radioactive source, and require the sample be placed within 2 mm of the detector assembly. Desktop units range in price from $60,000 to $80,000, depending on the capabilities. They require the sample to be placed about 1 cm from the detector assembly. "Process control" units are basically desktop units that have some automated features for handling samples, and more complex output options. Samples are typically fluids or wafers, and are not in vacuum. The lowest price "process control" units cost around $150,000.

If, rather than buying a complete system, components are purchased and assembled, then a number of issues must be addressed. The basic required components are an x-ray source (either a shuttered radioactive source, or an x-ray tube with mounting, power supply, cabling, and Be window vacuum fitting), an x-ray detector (with any required temperature control), pulse shaping amplifier, multichannel analyzer, computer, and computer interface. Careful thought is necessary when choosing source strength, system geometry, detector resolution, and detector size. These considerations are discussed below.

The sensitivity of XRF measurement CIGS composition is determined primarily by the measured count rate. The smaller the number of counts in the peak, the larger the relative uncertainty. In fact, the relative standard deviation in the number of counts in the fluorescent peak of interest, N, is $\frac{\sqrt{N}}{N}$. Thus, for example, if limiting the uncertainty in signal to 0.5% is desired, the peak of interest must contain at least 40,000 counts. The number of counts in the peak of interest depends on the x-ray source intensity, the sample yield, the detector solid angle and sensitivity, and the number of photons unintentionally lost in windows and other absorptive material.

The x-ray source is a major factor in establishing the measured count rate. Sources can be purchased in a variety of intensities, either as tubes or as radioactive sources. Tubes are advantageous because of their higher emissions, ability to turn off, lack of special licensing requirements, and excitation of lower energy lines (e.g. In Lα) via the continuous wavelength emission. Fluxes from typical x-ray tubes are usually over 3 orders of magnitude higher than those from the most intense radioactive sources commercially available[19,20]. Radioactive sources may be attractive for some applications because they are compact, low-cost, vacuum-compatible, and monoenergetic (reducing background and possibly simplifying quantification).

The sample yield is defined as the number of photons fluoresced from the sample in the peak of interest divided by the number of photons incident on the sample. For a 2.5 μm CIGS layer, with a Ga / (In + Ga) ratio of 0.25, and 20 keV incident x-rays, simulations show a sample yield for the Cu Kα peak of 3.8×10^{-3} photons fluoresced per incident photon. (Simulations were performed using the MRG simulation tool.)

If the emission of the x-ray source and the approximate fluorescence yield of the sample are known, only one more piece of information is needed to determine the counts per second that will be detected. This final piece of information is the portion of the source flux and the sample flux that will be utilized. In other words, for a given chamber geometry, one must know how much of the source's flux can be delivered to the substrate without illuminating non-sample items, and how much of the illuminated sample can be viewed by the detector with out picking up too much background. When the source and detector are very close to the substrate, the detector covers a large solid angle of the fluorescent flux, and the fraction of the source flux that is used in illuminating a given spot size on the sample is maximized. Counting rates are therefore largest when the source and detector are close to the sample. XRF measurements on CIGS modules may require slightly less source-to-sample and detector-to-sample proximity than average XRF applications, since large samples make a large spot size tolerable.

Using the information described above, Figure 14 shows the XRF count rate as a function of the distance from the sample to the source and detector. Count rate is shown for varying illuminated spot radii on the sample (i.e. varying degrees of source collimation). The calculations were performed for a 25 mCurie ^{109}Cd source illuminating a CIGS thin film, assuming an equal source-to-sample and sample-to-detector distance, and using typical detector size. Count rates are several orders of magnitude higher when an x-ray tube is used.

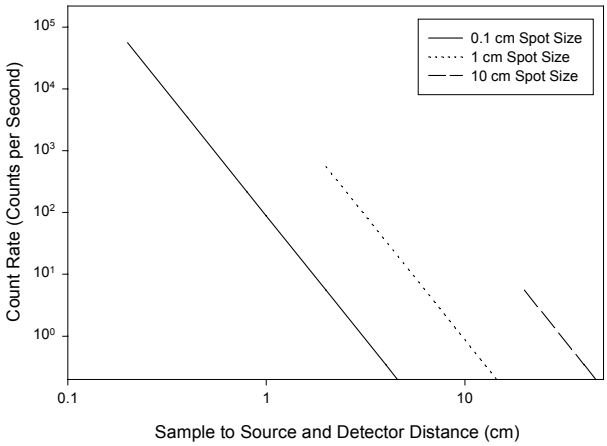

Figure 14: XRF Count rate as a function of distance from sample to radioactive source and detector.

The information discussed above can be used to calculate, for any desired precision, how close the source and detector need to be to the substrate. Suppose, for example, that the desired precision requires statistical errors are below 0.5%. Then, each peak measured must contain about 40,000 counts. If 90 seconds is an acceptable measurement time, the count rate must be at least 444 counts per second. Using Figure 14, the source and detector must be located no more than 2 cm from the substrate if a 1 cm spot radius is acceptable. The source and detector must be located no more than 0.9 cm from the substrate if a 0.1 cm spot radius is acceptable. Note that the above calculations assume that the light entering the detector is essentially uncollimated, and therefore some shielding to reduce the amount of background scatter from the chamber entering the detector will be required. Also note that typical acquisition times are on the order of tens of seconds (not milliseconds). Thus, if XRF is performed on a moving substrate, the measured composition is an average over the material that has passed under the beam during the measurement time. Maintaining high count rates while keeping sensing equipment removed from the deposition sources is a key challenge in implementing XRF in a CIGS deposition zone.

The basic design of the prototype XRF unit under construction is shown in Figure 15. Dimensions and components are chosen to provide acceptable count rates, energy resolution, and equipment costs for in-situ sensing of CIGS films. Necessary electronics were chosen to be computer-controllable, so that the sensor can be easily integrated into deposition chamber controls.

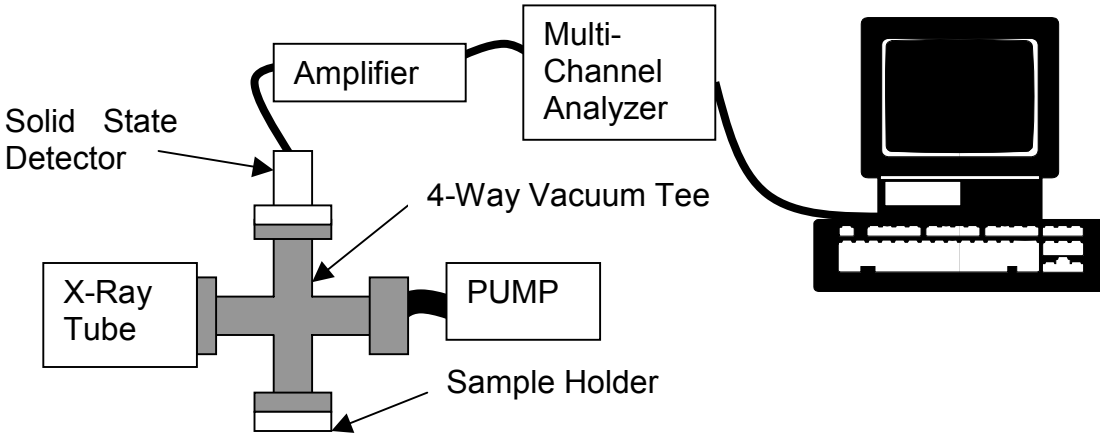

Figure 15: Basic design of XRF prototype under construction at MRG.

Inside the vacuum tee, the sample is held so that it is illuminated by x-rays, and so that fluoresced x-rays have an unobstructed path to the detector. Collimation is also included. At present, all sample-holding parts are planned to be made of Al, since fluorescence from Al is well-removed in energy from sample fluorescence lines. Later, when used in an Se-containing environment, the sample-holder and collimator will be made from an alternate material. Because

the system is mounted in vacuum, the attenuation of the lower-energy fluoresced radiation (e.g. In Lα x-rays) is minimized, and personnel are insured against exposure to x-rays.

The system shown in Figure 15 will not be used for depositions. Nonetheless, it will allow a number of necessary experiments. First, components have been chosen to allow a wide range of source-to-sample and sample-to-detector distances. Experiments will be performed to determine the minimum requirements on these distances and on sample size for a desired precision and measurement time. Second, the system will allow evaluation of hardware and software components before their installation in a manufacturing facility.

6. Se Sputtering

The evaluation of pulsed DC Se sputtering was proposed as a possible avenue to provide a high deposition rate, tightly controlled, low-cost method of Se delivery. Pulsed DC sputtering was believed to hold promise in these areas because, at MRG, sputter rate from insulating targets of other materials has been increased many fold at a given cathode power by sputtering the target in a pulsed DC, rather than RF, mode. The deposition rate during such processes can be tightly controlled by use of OES[21]. Additionally, the pulsed DC power supplies required to deposit at a given rate are much cheaper than their RF counterparts.

Pulsed DC sputtering of Se was performed. Deposition rate was examined as a function of chamber pressure, source-to-substrate distance, cathode power, and target thickness. The experiments described above were performed at a fixed pulsing frequency of 20 kHz, as dictated by the available equipment. A DC plasma (no pulsing) could not be maintained using the Se target. The best deposition rate achieved by pulsed DC sputtering was 0.5 Å/sec. The effect of annealing the Se target in the presence of In and Ga was also investigated. Such anneals have been reported to affect the crystallinity and doping of the target, and hence the conductivity and maximum deposition rate[22]. However, no measurable increase in target conductivity or in deposition rate was observed. Furthermore, no Se emission lines were observable in the plasma. The lack of detectable Se lines is presumably due to the small amount of Se in the plasma (i.e. small deposition rate), the absence of strongly emitting Se lines in the detectable range (240 to 1100 nm), and the strength of the Ar emissions.

Thus, it is concluded that pulsed DC sputtering of Se is not an attractive option for manufacturable CIGS. First, because of the lack of detectable Se lines in the plasma, OES cannot be used for deposition rate control of Se. Second, the 0.5 Å/sec deposition rate achieved is slightly smaller than that which has been achieved by RF sputtering[23],[24] and significantly smaller than deposition rates used when evaporating Se for use in CIGS solar cells[25]. Pulsed DC

sputtering does yield an advantage in equipment costs over RF sputtering when low deposition rates are acceptable, but higher deposition rates are necessary for manufacturable CIGS solar cells. Furthermore, it has been reported that a wide range of Se deposition rates are acceptable for the formation of good CIGS, due to the self-limiting nature of Se incorporation[26]. Thus, Se evaporation paired with traditional deposition rate monitors, such as quartz crystal monitors, most likely remains a necessary ingredient in the manufacture of CIGS solar cells.

7. CIS National Team Activities

The development of an XRF sensor for CIGS composition is consistent with NREL team goals set forth by industrial partners Energy Photovoltaics (EPV) and Global Solar Energy (GSE). MRG has taken a number of steps to insure that XRF development meets the industrial partners' needs. First, comments on required specifications for the sensor were solicited from representatives at GSE and EPV. Specifications discussed include required accuracy, acceptable measurement time, substrate motion during measurement, expected variations in the Mo back contact, materials safety issues, and required availability date of sensor. Second, upon request, MRG has provided a review of XRF principles, as well as information on XRF equipment and pricing, to both EPV and GSE. Third, a prototype versatile, low-cost, in-situ CIGS composition sensor has been designed. All components of this sensor are commercially available. The ultimate design of this sensor is likely to be a useful option for process control for the interested partners. Finally, MRG has agreed to measure samples from both industrial partners. These measurements will allow exploration of how XRF analysis must be adjusted for differing substrates, elemental gradients, and back contacts. MRG will continue to keep interested industrial partners updated and insure that developed technology meets their needs.

8. Conclusions

Materials Research Group (MRG), Inc. is developing in-situ sensors to improve yield, reproducibility, average efficiency, and prevention of "lost processes". In-situ x-ray fluorescence (XRF) will be used to monitor composition and thickness of deposited layers, and in-situ optical emission spectroscopy (OES) will be used to provide real-time feedback describing the deposition plasma. Characterization techniques are to be examined ex-situ in the first two years of the contract, and applied to existing deposition systems in the final year of the contract. Progress toward achieving these goals during Phase I includes

- development and verification of an XRF simulation tool to troubleshoot measurements, to predict difficulties in XRF interpretation, and to calculate quantities needed in the translation from XRF signal to composition;
- examination of the implication of sample conditions unique to CIGS photovoltaics - such as varying Ga gradients, intermediate film thicknesses

where neither thick-film nor thin-film approximations are valid, variations in back contact thickness, multiple layers, variations in substrate composition and thickness - on XRF interpretation;
- fabrication of CIGS samples and test structures for XRF measurements;
- execution and interpretation of XRF measurements examining system accuracy;
- design of a prototype XRF sensor built entirely of cost-effective, commercially available components that are suitable for integration into closed-loop deposition control;
- evaluation of pulsed DC sputtering of Se; and
- interaction with CIS National Team industrial partners to specify and adapt sensor functions.

9. Future Plans

A number of important items remain to be accomplished in Phases II and III. First, in the near future, the sources of the remaining Cu contamination in the LMA XRF system must be determined. It is suspected that eliminating this contamination will alter the observed disagreement between expected and measured Cu emission. XRF measurements will also be made on the prototype sensor assembled at MRG, and compared with the higher-resolution LMA measurements. After the effects of contamination are eliminated, and XRF signals from baseline samples can be shown to agree with the predicted values, the same relationships must be verified for more complicated samples, such as those containing Ga, or compositional gradients. The effect of varying substrates on the XRF signal must also be examined. Samples on various glasses, samples on polyimide, and samples made by the industrial partners - using their own back contacts and substrates - will be examined.

In the longer term, a number of issues involving real-time control will be addressed. A prototype XRF system will be installed on a CIGS deposition system, and composition and thickness information will be output to the chamber controls in real time. Information pertaining to the real-time XRF sensing of CdS, ZnO, and ITO will also be gathered. The relationships between deposition rates and plasma emissions of absorber and window materials will be obtained at MRG and LMA and used for closed-loop control.

10. References

[1] R.D. Weiting, *AIP Conference Proceedings* **353**, 19-25, (1995).
[2] K.E. Knapp, *AIP Conference Proceedings* **306**, 83-91, (1993).
[3] R. Muller, *Spectrochemical Analysis by X-Ray Fluorescence*, London: Adam Hilger, 1972, pg. 177.

[4] M. Murata, *X-Ray Spectrometry* **2**, 111-116 (1973).
[5] B. J. Mitchell, *Anal. Chem.* **32**, 1652-1657 (1960).
[6] J.W. Criss, L.S. Birks, *Anal. Chem.* **40**, 1080-1088 (1968).
[7] H.J. Beattie, R.M. Brissey, *Anal. Chem.* **26**, 980-989 (1954).
[8] R.J. Traill, G.R. Lachance, *Can. Spectrosc.* **11**, 63-69 (1966).
[9] R. Tertian, R. Vie le Sage, X-Ray Spectrom. 6, 123-130 (1977).
[10] W.K. de Jongh, *X-Ray Spectrom.* **2**, 151-158 (1973).
[11] R. Tertian, F. Claisse, *Principles of Quantitative X-Ray Fluorescence Analysis*, Heyden Publishing, pp. 51-69.
[12] J.W. Robinson, *CRC Handbook of Spectroscopy*, Vol. 1, 1974
[13] R. Tertian, F. Claisse, *Principles of Quantitative X-Ray Fluorescence Analysis*, Heyden Publishing, pp. 59-60.
[14] Ibid., pg 63.
[15] G.T. Bush, M.D. Stebel, "Measuring Plating Thickness with X-Ray Fluorescence", *Plating and Surface Finishing*, September 1983, pp. 80-84.
[16] R. Tertian, F. Claisse, *Principles of Quantitative X-Ray Fluorescence Analysis*, Heyden Publishing, pg. 64.
[17] M.A. Contreras, T.J. Gillespie, C.H. Marshall, T. Berens, R.N. Bhattacharya, D.L. Schulz, C.J. Curtis, K. Ramanathan, R. Noufi, "Fabrication Methods of Cu(In,Ga)Se_2 Polycrystalline Materials and Devices Currently Under Development at the National Renewable Energy
[18] T.D. McKinley, K.F.J. Heinrich, D.B. Wittry, *The Electron Microprobe*, John Wiley & Sons, Inc., New York, 1966, pg. 200 ff.
[19] R.E. Van Grieken, A. A. Markowicz, *Handbook of X-Ray Spectrometry: Methods and Techniques*, Marcel Dekker, Inc., New York, 1993, pg. 172.
[20] Isotope Products Laboratories, *Catalog of Products*, (818) 843-7000.
[21] I.L. Eisgruber, J.R. Engel, R.E. Hollingsworth, P.K. Bhat, R. Wendt, "Intelligent Process Control of Indium Tin Oxide Sputter Deposition Using Optical Emission Spectroscopy", *Journal of Vacuum Science and Technology A*, **17(1)**, 1999, pp. 190-197.
[22] Dr. Frank Kustas, private communication, November 2, 1998.
[23] Arya et al, 22nd Photovoltaics Specialists Conference, pg. 903, 1991.
[24] Nakada et al, 23rd Photovoltaics Specialists Conference, pg. 560, 1993.
[25] Hedstrom, H. Ohlsen, M. Bodegard, A. Kylner, L. Stolt, D. Hariskos, M. Ruckh, H.W. Schock, *Proceedings of the 23rd IEEE Photovoltaics Specialists Conference*, 364-371 (1993).
[26] J.R. Tuttle, M.A. Contreras, K.R. Ramanathan, S.E. Asher, R. Bhattacharya, T.A. Berens, J. Keane, R. Noufi, "Materials and Processing Issues in Thin-Film Cu(In,Ga)Se_2 Based Solar Cells", *AIP Conference Proceedings 394*, 83-105 (1996).

REPORT DOCUMENTATION PAGE

Form Approved
OMB NO. 0704-0188

1. AGENCY USE ONLY (Leave blank)	2. REPORT DATE	3. REPORT TYPE AND DATES COVERED
	September 1999	Annual Technical Report, 15 February 1998–15 February 1999

4. TITLE AND SUBTITLE
In-Situ Sensors for Process Control of CuIn(Ga)Se_2 Module Deposition; Annual Technical Report, 15 February 1998–15 February 1999

5. FUNDING NUMBERS
C: ZAK-8-17619-08
TA: PV905001

6. AUTHOR(S)
I.L. Eisgruber, T.L.Wangensteen, C. Marshall, B. Carpenter, R. Treece, R. Hollingsworth, G. Patel, J. Ogard, P.K. Bhat

7. PERFORMING ORGANIZATION NAME(S) AND ADDRESS(ES)
Materials Research Group, Inc.
12441 W. 49th Ave., Suite #2
Wheat Ridge, CO 80033-1927

8. PERFORMING ORGANIZATION REPORT NUMBER

9. SPONSORING/MONITORING AGENCY NAME(S) AND ADDRESS(ES)
National Renewable Energy Laboratory
1617 Cole Blvd.
Golden, CO 80401-3393

10. SPONSORING/MONITORING AGENCY REPORT NUMBER
SR-520-26382

11. SUPPLEMENTARY NOTES
NREL Technical Monitor: H.S. Ullal

12a. DISTRIBUTION/AVAILABILITY STATEMENT
National Technical Information Service
U.S. Department of Commerce
5285 Port Royal Road
Springfield, VA 22161

12b. DISTRIBUTION CODE

13. ABSTRACT *(Maximum 200 words)*

Materials Research Group (MRG), Inc., is developing in-situ sensors to improve yield, reproducibility, average efficiency, and prevention of "lost processes." In-situ X-ray fluorescence (XRF) will be used to monitor composition and thickness of deposited layers, and in-situ optical emission spectroscopy (OES) will be used to provide real-time feedback describing the deposition plasma. Characterization techniques are to be examined ex-situ in the first two years of the contract, and applied to existing deposition systems in the final year. Progress toward achieving these goals during Phase I includes:

- Development and verification of an XRF simulation tool to troubleshoot measurements, to predict difficulties in XRF interpretation, and to calculate quantities needed in the translation from XRF signal to composition;
- Examination of the implication of sample conditions unique to CIGS photovoltaics - such as varying Ga gradients, intermediate film thicknesses where neither thick-film nor thin-film approximations are valid, variations in back-contact thickness, multiple layers, variations in substrate composition and thickness - on XRF interpretation;
- Fabrication of CIGS samples and test structures for XRF measurements;
- Execution and interpretation of XRF measurements examining system accuracy;
- Design of a prototype XRF sensor built entirely of cost-effective, commercially available components that are suitable for integration into closed-loop deposition control;
  Evaluation of pulsed DC sputtering of Se; and
- Interaction with CIS National Team industrial partners to specify and adapt sensor functions.

14. SUBJECT TERMS
photovoltaics ; X-ray fluorescence ; XRF ; CIGS ; optical emission spectroscopy ; OES ; sample fabrication ; in-situ sensors ; process control ; module deposition

15. NUMBER OF PAGES
32

16. PRICE CODE

17. SECURITY CLASSIFICATION OF REPORT	18. SECURITY CLASSIFICATION OF THIS PAGE	19. SECURITY CLASSIFICATION OF ABSTRACT	20. LIMITATION OF ABSTRACT
Unclassified	Unclassified	Unclassified	UL